J. Fluid Mech. (1998), *vol.* 358, *pp.* 177–202. Printed in the United Kingdom

An experimental study of oblique transition in plane Poiseuille flow

By PER A. ELOFSSON AND P. HENRIK ALFREDSSON

Department of Mechanics, Royal Institute of Technology, S-100 44 Stockholm, Sweden

(Received 22 July 1996 and in revised form 27 October 1997)

Interactions of oblique waves have recently been investigated theoretically and numerically and found to give rise to rapid transition in flows subcritical to linear wave disturbances. The transition scenario consists of the formation and transient growth of streamwise streaks of high and low velocity and later a rapid growth of high-frequency disturbances leading to breakdown. The present study is the first extensive experimental investigation of oblique transition. The experiments were carried out in a plane Poiseuille flow air channel in which the oblique waves were generated, one at each wall, by vibrating ribbons and the development of the flow was mapped with hot-wire anemometry. The experiments consist both of low- and high-amplitude wave disturbances; in both cases streaky structures are created. For the low-amplitude case these structures decay, whereas for the high amplitude the flow goes towards breakdown. This study has confirmed and extended previous theoretical and numerical results showing that oblique transition may be an important transition scenario.

1. Introduction

Transient growth has been shown to be a possible linear mechanism for the growth of three-dimensional disturbances at subcritical Reynolds numbers in wall-bounded flows. In the inviscid case Ellingsen & Palm (1975) and Landahl (1980) showed that a three-dimensional disturbance may grow algebraically with time if there is a forcing by the normal velocity. For plane Poiseuille flow Gustavsson (1991) showed that after the initial algebraic growth, the disturbance energy reaches a maximum after which it decays due to viscosity. He also showed that the time scale for growth scaled with the Reynolds number, i.e. the time to reach a certain size is proportional to Re^{-1} ($Re = U_{CL}h/\nu$, where U_{CL} is the laminar centreline velocity, h is half the channel height and ν is the kinematic viscosity). For infinitely long disturbances Gustavsson found the largest amplification to occur for spanwise wavenumbers close to $\beta = 2$ ($\beta = 2\pi h/\lambda$, where λ is the spanwise wavelength), although the wavenumber dependence was not very strong. Butler & Farrell (1992) extended this work by determining the optimal perturbation for plane Poiseuille and Couette flow as well as for a (parallel) Blasius boundary layer flow. A summary of the development up to this point can be found in Trefethen *et al.* (1993). It should be pointed out (*e.g.* see Waleffe 1997) that transient growth of streaky structures is only the first step towards transition, the latter stages must involve nonlinear effects.

All the above studies view transient growth as a temporal process; however in most physical flows disturbances develop in space instead of time. There is no clear-cut way to transform the temporal results to the spatial development, but several experiments (both numerical and physical) show that a similar development can occur spatially,

i.e. as the disturbance moves downstream its energy may first increase, whereas viscous decay will eventually make it disappear. However, if the disturbance amplitude becomes large enough the structure may instead break down into turbulence.

One example is the experiment by Klingmann (1992) who investigated growing three-dimensional disturbances in plane Poiseuille flow at subcritical Reynolds numbers. She used a point-like disturbance which developed into streaky structures. The energy of the structure first increased linearly, whereupon, depending on the strength of the initial disturbance, it either decayed or gave rise to a turbulent spot. This scenario seems to be close to what is described by the temporal analysis. Henningson, Lundbladh & Johansson (1993) made direct numerical simulations of the same flow with a localized disturbance which further corroborated the transient growth mechanism. It is noteworthy that one old transition experiment has been re-evaluated and evidence for the existence of transiently growing disturbances was found (see Mayer & Reshotko 1997). In the analysis the temporal development was converted to a spatial development by using the propagation velocity of the disturbance.

A theoretical analysis of transient growth in a spatial context has been presented by Luchini (1996) for boundary layer flow. He has shown the existence of three-dimensional self-similar solutions (i.e. streaky structures) where the streamwise disturbance velocity grows as $x^{0.213}$. Hence in spatially growing boundary layer flows it is not necessary true that transient growth will be followed by viscous decay. Therefore the transient growth mechanism may be quite important for boundary layer transition in the case of excitation by three-dimensional disturbances (such as localized roughness elements or free-stream turbulence).

1.1. *Oblique transition*

The oblique transition concept was introduced by Schmid & Henningson (1992) and involves transient growth as a major component. The starting point is the introduction of two oblique waves of small but finite amplitude. The wave pair can be characterized by $(\omega_0, \pm\beta_0)$, where ω_0 is their angular frequency and $\pm\beta_0$ their spanwise wavenumbers. They may interact nonlinearly and formally one can state that the first-generation interaction will give components characterized by (0,0), $(2\omega_0,0)$, $(2\omega_0, \pm 2\beta_0)$ and $(0, \pm 2\beta_0)$, where the fourth corresponds to a stationary, spanwise-periodic disturbance. It was found by Schmid & Henningson that initially the $(0, \pm 2\beta_0)$ mode reaches high amplitudes through transient growth. The result is a streaky structure in the streamwise velocity, which was verified experimentally in plane Poiseuille flow by Elofsson & Alfredsson (1995).

Berlin, Lundbladh & Henningson (1994) carried out direct numerical simulations of oblique transition in a Blasius boundary layer flow (i.e. the initial disturbance was two oblique waves) and found that after an initial growth of the streaky structures a rapid growth of modes with non-zero ω followed. Later Wiegel (1996) showed the existence of oblique transition in flat-plate boundary layer experiments. Berlin *et al.* (see also Lundbladh *et al.* 1994) suggested that oblique transition consists of the following three stages: firstly, nonlinear generation of streamwise vortices by a pair of oblique waves (which can be understood by considering the forcing of the streamwise vorticity by nonlinear terms resulting from the pair of oblique waves, see the Appendix for details); secondly transient growth of streaks; and thirdly, breakdown of the flow due to a secondary instability of the streaks provided their amplitude exceeds a threshold amplitude. This last stage has recently been investigated by Reddy *et al.* (1998) who studied the secondary instability of streaks in plane channel flows through direct numerical simulations and stability calculations. Their results indicate

that the secondary instability is mainly due to spanwise inflectional profiles which occur through the transient growth of the streaky structures. A similar analysis was made by Waleffe (1997) whose main purpose was to study streak instability as one part of a process describing self-sustained turbulence near walls.

1.2. *Transition originating from Tollmien–Schlichting waves*

An alternative route to transition is the widely studied scenario which considers growing two-dimensional waves which become three-dimensional and break down to turbulence. The linear stage is known to be described by the Orr–Sommerfeld equation and the travelling wave disturbances which develop according to this equation are denoted Tollmien–Schlichting (TS-) waves. The experimental verification of such waves was reported by Schubauer & Skramstad (1947) where the waves were generated by a vibrating ribbon close to the surface of a smooth plate in a wind tunnel with a low free-stream turbulence level. Almost perfect agreement between the linear parallel theory and experimental results on two-dimensional waves was finally obtained by Klingmann *et al.* (1993) in the case of the Blasius boundary layer. Their results showed that non-parallel effects were small in the case of two-dimensional waves, in contrast to several previous investigations.

Also, oblique waves have been found to follow linear theory. Gaster (1975) was able to simulate the growth of a wave packet by linear theory, whereas Kachanov & Michalke (1994) made an extensive study of among other things the growth rate for oblique waves.

For the TS-wave transition scenario the two-dimensional waves develop a strongly growing three-dimensionality which leads to breakdown. This can be modelled by considering a combination of a two-dimensional wave with small-amplitude oblique waves. Klebanoff, Tidstrom & Sargent (1962) reported on one such scenario which results in an aligned pattern of Λ-vortices and is usually denoted K-transition (K for Klebanoff). Another secondary instability scenario, the so-called subharmonic-mode breakdown (see Kachanov & Levchenko 1984) results in the formation of staggered Λ-vortices which hence gives rise to a subharmonic frequency. The TS-wave scenario has been thoroughly investigated in experiments, see e.g. Corke & Mangano (1989) who performed measurements on controlled two-dimensional and three-dimensional disturbances in a flat plate boundary layer flow. The studies cited above concerned the boundary layer flow developing on a flat plate at zero pressure gradient, and which of the described scenarios (fundamental or subharmonic) that will dominate in a situation is strongly dependent on the amplitudes of the TS-wave and the oblique waves.

In plane Poiseuille flow transition usually occurs at Reynolds numbers for which two-dimensional TS-waves are damped. Despite the fact that the waves are damped they can still undergo a secondary instability forced by three-dimensional disturbances. In experimental investigations where the two-dimensional waves were artificially forced the breakdown has been observed under various conditions (sub- and supercritical Reynolds numbers) to be of K-type, see for instance Nishioka, Iida & Ichikawa (1975). In these experiments the three-dimensionality was provided through a non-uniform basic flow. These observations are in contrast to the theory of Herbert (1983) which predicts subharmonic transition to dominate for small TS-wave amplitudes. A possible explanation was given by Singer, Reed & Ferziger (1989), who used direct numerical simulations to study the effect of weak streamwise vortices. They found that the presence of streamwise vortices caused K-type transition to dominate even at conditions for which theory predicts the dominance of subharmonic modes. The different transition scenarios have also been investigated by Saiki *et al.* (1993)

through spatial numerical simulations at $Re = 5000$. In all these cases the two-dimensional wave has a fairly high amplitude which could not be realized naturally if the flow is subcritical.

1.3. *Motivation of present work*

From what has been described above it seems clear that oblique transition is qualitatively different from the traditional TS-wave scenario. In oblique transition the starting point is the interaction of two small- but finite-amplitude oblique waves. This is in contrast to the models describing the secondary instability of two-dimensional TS-waves where two small-amplitude oblique waves gain energy from their interaction with the mean flow and a finite amplitude two-dimensional wave. Also the later stages before breakdown are quite different: in oblique transition the transiently growing streaks seem to undergo a spanwise inflectionally induced secondary instability whereas the TS-wave route to transition involves the formation of Λ-shaped structures. It is clear that the TS-wave scenario may dominate in the boundary layer case since transition usually is supercritical. It is more questionable whether this scenario is responsible for unforced transition in various types of channel flows which occur at subcritical Reynolds numbers. This is also substantiated by Henningson (1995) and Reddy *et al.* (1998) who have shown that the energy of a two-dimensional wave has to be almost three orders of magnitude larger than that of a pair of oblique waves to cause subcritical transition in plane Poiseuille flow at $Re = 2000$.

The main purpose of the present investigation was to verify the proposed oblique transition scenario in a physical experiment. In § 2 we describe the experimental procedure and characterize the base flow and also the method for the linear stability calculations is presented. Section 3 contains the results from the initial investigations on the characteristics of two-dimensional and oblique waves. These results show that it is possible to generate both types of waves in plane Poiseuille flow with the technique of vibrating ribbons. It also gives new and extended experimental observations of linear stability in plane Poiseuille flow. The main part of the present work is contained in § 4 where the oblique transition results are described. Two cases are discussed: first a small- but finite-amplitude case where the interaction of the waves gives rise to streaky structures which after an initial transient growth decays and transition do not occur; and secondly, a high-amplitude case where the interaction also results in streaky structures, but where the amplitude of the streaks becomes much larger and the structures finally break down. Finally, § 5 contains further discussion and a summary of the main findings.

2. Experimental description

2.1. *Set-up*

The experiments were performed in an air-flow channel at the Royal Institute of Technology (KTH). The channel is a modified version of the one used by Klingmann (1992). The channel consists of two 10 mm thick glass plates separated by 8.2 mm thick distance bars of aluminium which are positioned to give a channel width of 830 mm (see figure 1). Air is taken from the room and a frequency-controlled fan forces it to the settling chamber through a perforated distribution pipe and two screens followed by guide vanes and a package of three damping screens. After passing the settling chamber the air flows through a 40 : 1 ratio contraction before it enters the 1.9 m long channel. The channel is equipped with static pressure taps and a total pressure probe for calibration and monitoring purposes.

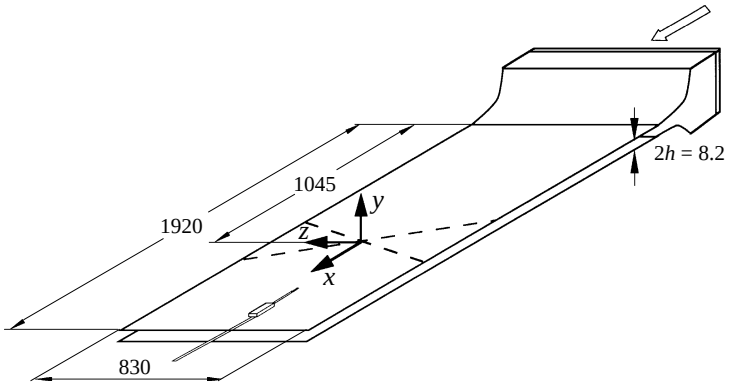

FIGURE 1. Experimental set-up. All measurements in mm.

Measurements of the streamwise velocity component were made using an AA-systems 1003 constant-temperature anemometer and platinum single-wire probes having a wire diameter and length of 2.5 μm and 0.5 mm, respectively. The hot-wire probe is mounted to a wedge-manouverable mechanism which allows the probe to be traversed in a direction normal to the channel walls. The wedge mechanism is mounted on an aluminium bar which can be moved in the streamwise and spanwise direction by means of two perpendicular guide systems. Stepping motors mounted to the wedge rod and the spanwise guide system make it possible to automatically traverse the hot-wire probe in the wall-normal and spanwise directions with a minimum step of 0.015 mm and 0.05 mm, respectively. A Macintosh computer and a MacADIOS adio I/O unit were used for controlling the stepping motors and the data acquisition.

The hot-wire probe was calibrated against the parabolic Poiseuille profile at a position 40 half-channel heights (h) downstream of the ribbons, which are mounted $255h$ downstream of the channel entrance. The calibration curve used was

$$U = k_1(E^2 - E_0^2)^{1/n} + k_2(E - E_0)^{1/2}, \tag{2.1}$$

where E is the anemometer voltage at the velocity U, E_0 the voltage at zero velocity and the coefficients k_1, k_2 and n are determined from a best fit of the data to the calibration function. Typically the calibration procedure resulted in an error of less than 0.7% for all calibration points.

In the following velocities are normalized with the laminar centreline velocity U_{CL} and lengths are normalized with the half-channel height, $h = 4.1$ mm. The co-ordinate system has the x-axis aligned in the streamwise, the y-axis in the wall normal and the z-axis in the spanwise direction. The origin is at the crossing point for the two ribbons and half-way between the lower and the upper plate.

2.2. *Characteristics of the mean flow*

Measurements were made to characterize the base flow in the channel, both with and without the ribbons mounted inside the channel. The maximum background disturbance level was found to be 0.16% for the case with $Re = 2000$ and both ribbons mounted inside the channel without being forced. For a Reynolds number of 2000 a fully developed parabolic profile is obtained at approximately $220h$ downstream of the channel entrance, see Schlichting (1979, p. 186). Figure 2 shows mean velocity profiles across the channel measured at different streamwise positions with the two ribbons mounted inside the channel but without being forced. Experimental data are

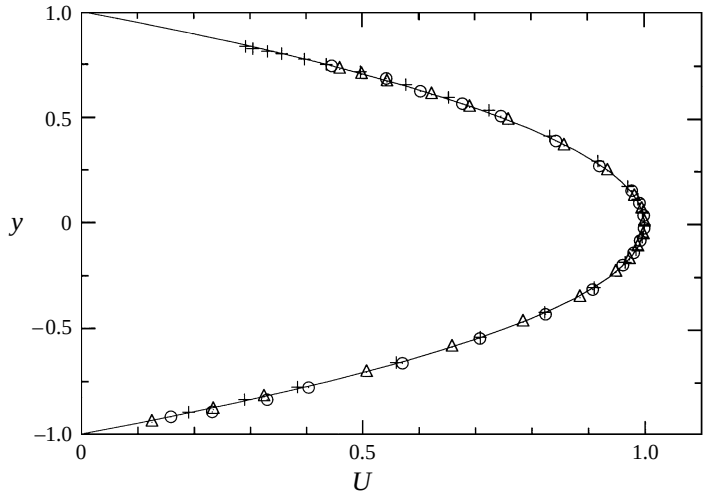

FIGURE 2. Base flow with ribbons mounted inside the channel, $Re = 2000$ and $z = 0$. Measurements at: ○, x=5; +, x=50; △, x=100; — corresponds to the parabolic profile.

shown as symbols and the line is the parabolic velocity profile. The velocity profile at $x = 5$ is slightly distorted near the y-positions where the ribbons are mounted ($y = \pm 0.88$), but the profiles which are measured further downstream do not indicate any influence from the ribbons. The spanwise uniformity was also investigated and the deviation in U_{CL} was found to be less than $\pm 0.3\%$ at the centreline $40h$ downstream of the ribbon intersection.

When traversing the hot-wire probe in the streamwise direction the centreline velocity was found to change slightly, and its value increased by 1 % when the hot-wire probe was traversed from the ribbon intersection to a position $70h$ downstream. This change is believed to be an effect of the turbulent wedges that develop along the channel sides which gives rise to a blockage of the flow. Also the traversable guide bar which supports the hot wire gives rise to a pressure drop in the channel which decreases when it is moved downstream and hence the flow rate may become larger causing an increase in the centreline velocity.

2.3. *Wave generation procedure*

In the present study wave disturbances were generated with vibrating ribbons. Different ribbon arrangements were used with either a single ribbon mounted at the lower wall or one ribbon at each channel wall. The ribbons were made of phosphorus bronze and had a width and thickness of 3 mm and 0.05 mm, respectively. Each ribbon spanned the whole channel width but only the central 320 mm of each ribbon was vibrating. The working length of the ribbon and the distance between ribbon and channel wall was set by 0.5 mm thick aluminium spacers positioned between the ribbon and the glass wall. The tension of the ribbon was adjusted with a mechanism mounted on one of the ribbon ends. After the ribbon tension had been adjusted the part of the ribbon that was not vibrating was firmly attached to the channel wall by a thin tape. Five permanent horseshoe magnets were placed along each ribbon on the outside of the channel and the ribbon was made to vibrate by supplying it with a sinusoidal electrical current. The forcing signal was provided by a function generator and thereafter amplified by an audio amplifier whose output was connected to a power resistor and a 220/33 V transformer. The amplitude of the signal to the

ribbon was adjusted with a precision potentiometer connected between the function generator and the input of the amplifier.

2.4. *Procedure and dataprocessing*

Most of the measurements were made at a Reynolds number $Re = 2000$ ($U_{CL} \approx 7.3$ m s^{-1}) and with the ribbons oscillating at an angular frequency $\omega \approx 0.34$ ($\omega = 2\pi f h/U_{CL}$) which corresponds to a dimensional frequency close to 96 Hz. Some measurements were also made at $Re = 1600$ and at frequencies of oscillation in the range $\omega \approx 0.3$–0.5.

To describe the measurement results we decompose the velocity field $U(x, y, z, t)$ in a time-averaged part $\overline{U}$ and a fluctuating part u:

$$U(x, y, z, t) = \overline{U(x, y, z)} + u(x, y, z, t). \tag{2.2}$$

For the stationary disturbance field we use U_d defined as

$$U_d = \overline{U(x, y, z)} - \frac{1}{z_1 - z_0} \int_{z_0}^{z_1} \overline{U(x, y, z)}\, \mathrm{d}z, \tag{2.3}$$

where z_0 and z_1 are the spanwise limits of the measurement region. Two root-mean-square (r.m.s.) measures for time-dependent disturbances (u) will be used: both the total r.m.s., $u_{r.m.s.}$ and the r.m.s. obtained by filtering the signal in a 4 Hz band around the forcing frequency, $u_{r.m.s.,f_0}$.

The ribbons were adjusted to give the same maximum $u_{r.m.s.,f_0}$ in the lower and upper part of the channel at $x = 12$ and $z = 0$. During the measurements the forcing signals, the input signals to the ribbons, the static pressure drop and the temperature were monitored. For small deviations from the calibration temperature the anemometer voltage was compensated and if the temperature inside the channel deviated more than 0.5 °C from the calibration temperature the hot wire was recalibrated.

Phase information for the signals was obtained with a phase alignment procedure similar to the one used by Boiko *et al.* (1994). The hot-wire signal and the output from the function generator were sampled almost simultaneously. The timeshift of 35 μs was due to the limited throughput of the A/D-converter. By ensemble averaging the phase-aligned signals the random phase contributions were effectively cancelled out.

2.5. *Linear stability calculations*

By assuming oblique wave disturbances,

$$v = \hat{v}(y)\mathrm{e}^{\mathrm{i}(\alpha x + \beta z - \omega t)}, \tag{2.4}$$

one can derive the following form of the Orr–Sommerfeld equation:

$$[\mathrm{i}R(\alpha U - \omega)(\mathrm{D}^2 - k^2) - \mathrm{i}\alpha U'' + (\mathrm{D}^2 - k^2)^2\,]\hat{v} = 0. \tag{2.5}$$

In the following we will use the spatial formulation of the stability theory and hence $\alpha = \alpha_r + \mathrm{i}\alpha_i$ is a complex streamwise wavenumber, where α_r is the physical streamwise wavenumber and α_i gives the amplification of the wave; β is the spanwise wavenumber, $k^2 = \alpha^2 + \beta^2$ and ω is the angular frequency of oscillation. The phase velocity of the wave is defined as $c = \omega/\alpha_r$. With a wave angle formulation k^2 can be written as $k^2 = \alpha^2 + \alpha_r^2 \tan^2\phi$, where $\tan\phi = \beta/\alpha_r$. By choosing the boundary conditions, $\hat{v}' = \hat{v}''' = 0$ at the centreline ($y = 0$) and $\hat{v} = \hat{v}' = 0$ at the wall ($y = 1$) symmetric eigenfunctions $\hat{v}$ will be obtained, including the least stable one.

The eigenfunction $\hat{v}$ is obtained with a shooting method which uses a fourth-order Runge–Kutta scheme and an orthonormalization procedure. Typically 200 integration

steps are used when integrating from the centreline to the channel wall. After $\hat{v}$ has been determined the streamwise eigenfunction $\hat{u}$ can be obtained by integrating the following equation:

$$\left[\mathrm{D}^2 - k^2 + \mathrm{i}\alpha R\left(U - \frac{\omega}{\alpha}\right)\right]\hat{u} = R\left(1 - \frac{\alpha^2}{k^2}\right)U'\hat{v} + \left[R\frac{\alpha^2}{k^2}\left(U - \frac{\omega}{\alpha}\right) - \mathrm{i}\alpha\right]\hat{v}' + \mathrm{i}\frac{\alpha}{k^2}\hat{v}''', \tag{2.6}$$

with the boundary conditions, $\hat{u} = 0$ at the centreline ($y = 0$) and $\hat{u} = 0$ at the wall ($y = 1$). The solution is determined by combining the solution of the homogeneous problem and the particular solution in such a way that the boundary condition at the wall is fulfilled. When comparing with experimental data the absolute value $|\hat{u}|$ and the phase $\varphi = \arctan[\mathrm{Im}(\hat{u})/\mathrm{Re}(\hat{u})]$ are used.

3. Linear TS-wave development

In order to ascertain that the vibrating ribbons were working properly initial measurements were carried out with only one vibrating ribbon. Both two-dimensional and oblique waves were investigated and the ribbons were either mounted parallel to or inclined by 34° or 45° with respect to the spanwise direction. Amplitude and phase distributions across the channel of the streamwise disturbance velocity were measured at different streamwise and spanwise positions. Also, damping rates and phase evolutions were determined for various Re and ω.

3.1. *Two-dimensional TS-waves*

In this section experimental results for $Re = 1600$ will be compared with linear stability theory (see also § 2.5). Wave disturbances were generated by a vibrating ribbon mounted at the lower channel wall perpendicular to the streamwise direction. The ribbon was operated at an angular frequency $\omega = 0.42$ and a low amplitude was chosen in order for the waves to develop according to linear stability theory.

Figure 3 shows the amplitude and phase distributions measured at $x = 20$ and $z = 0$ for a maximum $u_{r.m.s.,f_0} = 0.25\%$ close to the ribbon ($x = 12$). The amplitudes have been normalised with their maximum values and when compared with linear theory (the line in figure 3) the overall agreement is seen to be good. The maxima in both the lower and upper parts of the channel are located at a distance of $0.2h$ from the walls; however, the maximum amplitude is about 10% smaller in the upper channel half than in the lower. This is probably because it takes some distance for the wave generated at the lower wall to reach the same amplitude in both channel halves. The phase distribution of u shows the characteristic phase shift of 180° at the centreline due to the opposite symmetries of u and v. The measured and calculated phase distributions were matched at $y = -0.35$. In contrast to the amplitude distribution the phase seems to adhere equally well to linear theory on both sides of the centreline, although there is a small deviation from linear theory close to the wall. In the spanwise direction the variation in the maximum value of $u_{r.m.s.,f_0}$ was $\pm 3\%$ over the central $16h$.

In figure 4 the amplitude and phase evolution for a wave disturbance at the same Re and ω as above are shown. For comparison results from linear theory are also displayed in the figure, corresponding to $\alpha_i = 0.043$ and $c = 0.35$, and the matching between measurements and calculations was done at the first measurement position ($x \approx 12$). The amplitude displayed in figure 4 (a) was determined by traversing the hot-wire probe normal to the wall in the lower part of the channel and then extracting

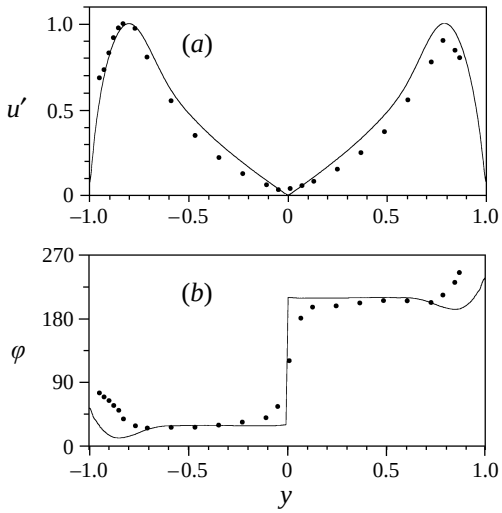

FIGURE 3. Tollmien–Schlichting wave at $Re = 1600$ and $\omega = 0.42$. (*a*) Wall-normal profile of amplitude ($u_{r.m.s.,f_0}$); (*b*) corresponding phase profile. •, Measurements at $x = 20, z = 0$; ——, results from linear stability theory.

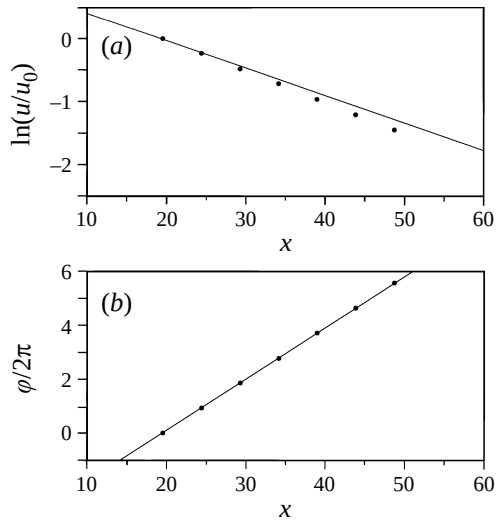

FIGURE 4. Tollmien–Schlichting wave at $Re = 1600$ and $\omega = 0.42$. (*a*) Development of amplitude ($u_{r.m.s.,f_0}$); (*b*) phase evolution. •, Measurements; ——, results from linear stability theory.

the maximum $u_{r.m.s.,f_0}$ for each streamwise position. The experimental data indicate a slightly larger damping rate than the results from linear stability theory, which may be due to the non-symmetry with respect to the two walls seen in the amplitude distribution. It should, however, be pointed out that the low disturbance amplitude makes it difficult to measure the amplitude with high accuracy especially for the points far from the ribbons. For the phase evolution (figure 4*b*) the agreement between the experimental results and linear theory is good (the phase was also determined at the maximum in the lower part of the channel).

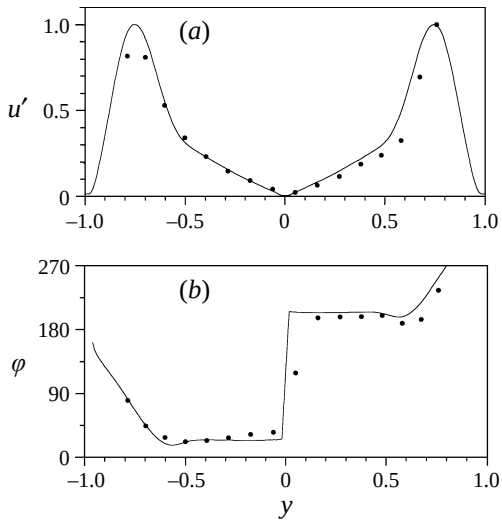

FIGURE 5. Oblique wave ($\phi = 45°$) at $Re = 2000$ and $\omega = 0.33$. (a) Wall-normal profile of amplitude ($u_{r.m.s.,f_0}$); (b) corresponding phase profile. •, Measurements at $x = 35, z = 0$; ——, results from linear stability theory.

3.2. *Oblique waves*

Oblique waves were generated by mounting one ribbon on the lower channel wall at an oblique angle to the direction of the flow. Wave disturbances with $\omega = 0.33$ were investigated at $Re = 2000$ and at a wave angle of 45°. As for the two-dimensional waves, a low initial amplitude is shown ($u_{r.m.s.,f_0} = 0.45\%$ at $x = 12$).

Figure 5(a) shows the amplitude distribution from measurements at $x = 35$ and $z = 0$. It is seen that linear theory and the experimental results are in close agreement. However, due to a limited number of measurement positions in the wall-normal direction it is not clear whether the maximum in the upper channel half is captured or not.

Also, the experimentally determined phase distribution and the one obtained from linear theory are in close agreement (figure 5b). Generally it is observed that oblique waves have their maxima in u further from the walls than two-dimensional waves at the same Re and ω. A comparison with figure 3(a) shows that this is the case: in figure 5(a) the maxima are located $0.25h$ from the walls, despite Re being higher (which leads to a shift of the maximum closer to the wall). It should also be noted that linear theory predicts that the oblique waves have small local maxima very close to the walls. (These maxima are e.g. shown in Zang & Krist (1989) for a supercritical $Re = 8000$.) The phase distribution on both sides of the centreline is characterized by a region of constant phase, but for the oblique wave this region is smaller and the deviation from this value close to the wall is larger than for the two-dimensional case.

The downstream amplitude and phase evolution are shown in figure 6. When comparing with the amplitude evolution for the TS-waves (figure 4) the evolution for the oblique waves displays a larger scatter but the data agree well with the result of linear theory ($\alpha_i = 0.044$). The measured downstream phase development gives a streamwise phase velocity of $c = 0.39$ which is close to the one given by linear theory, $c = 0.37$.

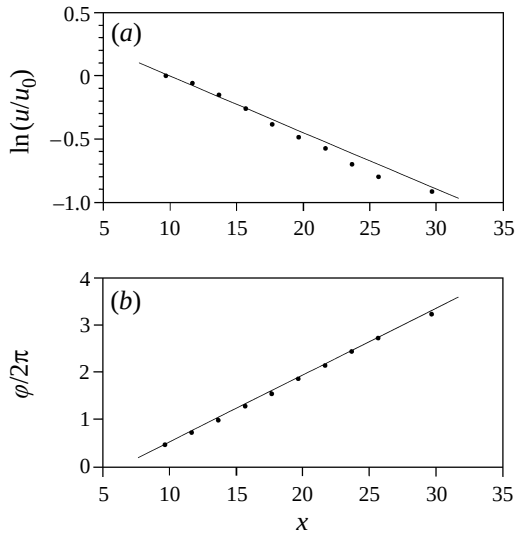

FIGURE 6. Oblique wave ($\phi = 45°$) at $Re = 2000$ and $\omega = 0.33$. (*a*) Development of amplitude ($u_{r.m.s.,f_0}$); (*b*) phase evolution. •, Measurements; ——, results from linear stability theory.

4. Oblique transition

The main aim of this study was to experimentally investigate the theoretically predicted transition scenario known as 'oblique transition' in various parameter ranges. Plane Poiseuille flow is an ideal flow field to carry out such an experimental study with vibrating ribbons as it is possible to generate one wave at each wall. In the present experiments, two oblique waves with the same angular frequency were generated, each making the same angle to the mean flow but with opposite sign. Two different wave angles were chosen, namely 34° and 45°, where the latter allowed us to make direct comparisons with results from numerical simulations. Two different ranges of amplitudes of the initial waves were used: a low range with initial amplitudes below 2.5% and a high range with amplitudes above 4%. The difference between the two was that for amplitudes below 2.5% transition did not occur within the experimental channel ($x \leqslant 200$) whereas for amplitudes in the high range transition took place within $70h$ from the intersection of the ribbons.

4.1. *Low-amplitude results*

Figure 7 shows the result of the interaction of two oblique waves of low amplitude. The measurements were made at $y = -0.75$ by traversing the hot wire in the spanwise direction in steps of 1.0 mm and in the streamwise direction in steps of 16.4 mm ($4h$). The original waves were generated at an angle of 45° with $\omega = 0.33$ and an initial maximum $u_{r.m.s.,f_0}$ of 1.5%. The figure shows contour plots of U_d, $u_{r.m.s.}$ and $u_{r.m.s.,f_0}$ in an (x, z)-plane (for definitions see § 2.4).

The longitudinal structures are strikingly illustrated by figure 7(*a*) where two full regions of high velocity and two of low velocity are seen. In the centre the structures have developed at $x = 20$ and their amplitude increases in the downstream direction to reach a maximum of $\pm 3.5\%$ inside the measurement area. The spanwise wavelength is approximately $3.4h$ corresponding to a wavenumber of 1.85 which is close to twice the spanwise wavenumber of the oblique waves (± 0.90). By traversing the hot-wire

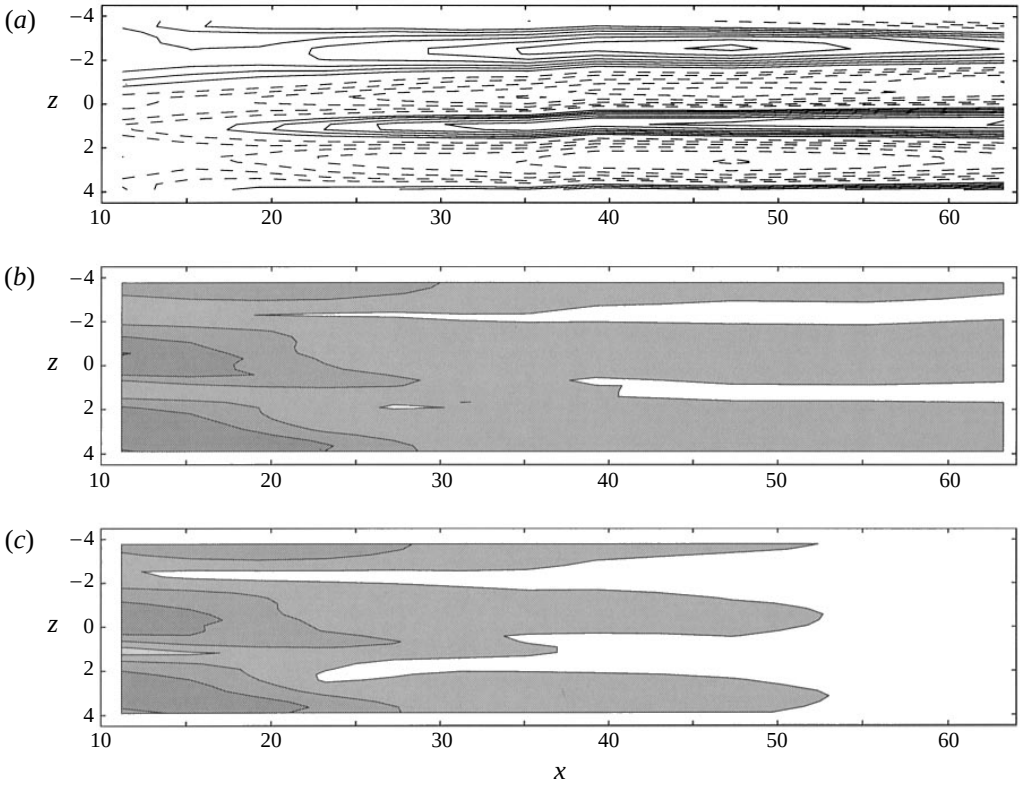

FIGURE 7. Contour plots in a streamwise–spanwise plane at $y = -0.75$, $Re = 2000$, $\omega = 0.33$ and $\phi = 45°$. (*a*) U_d, contours: $\pm 0.5\,\%$, $\pm 1\,\%$..; (*b*) $u_{r.m.s.}$, contours : 0.25%, 0.75%..; (*c*) $u_{r.m.s.,f_0}$, contours : 0.25 %, 0.75 %... Negative contours are dashed.

probe in the spanwise direction at $x \approx 125$ and studying the anemometer output, the spanwise structure with low- and high-velocity regions was clearly observed at this streamwise position also although the streak amplitude was less than the maximum values seen in figure 7 (*a*).

As can be observed in figure 7 (*b*) $u_{r.m.s.}$ decreases in the downstream direction and has its lowest amplitude in the high-velocity regions. The amplitude of the fundamental frequency (figure 7 *c*) also decays from a value slightly above 1.25% and the development is similar to that of $u_{r.m.s.}$.

When viewed in a cross-stream plane (figure 8) the distribution of regions with positive and negative U_d across the channel is clearly seen. Each region of low and high velocity is confined to either the upper or lower part of the channel and the maximum disturbance occurs close to $y = \pm 0.75$ although a slight shift towards the centreline is observed as the flow develops downstream. It is also clear that the picture displays a non-symmetry with respect to the spanwise centreplane, $z = 0$. The low- and high-velocity regions in the lower channel half appear to be shifted approximately $0.9h$ in the spanwise direction with respect to the regions above the centreplane. For an ideal situation where one introduces a symmetric pair of Orr–Sommerfeld modes the flow would become symmetric with respect to $y = 0$. In the experiment a non-symmetry is introduced since the waves are generated at different walls, which is also confirmed by the numerical simulations of Elofsson &

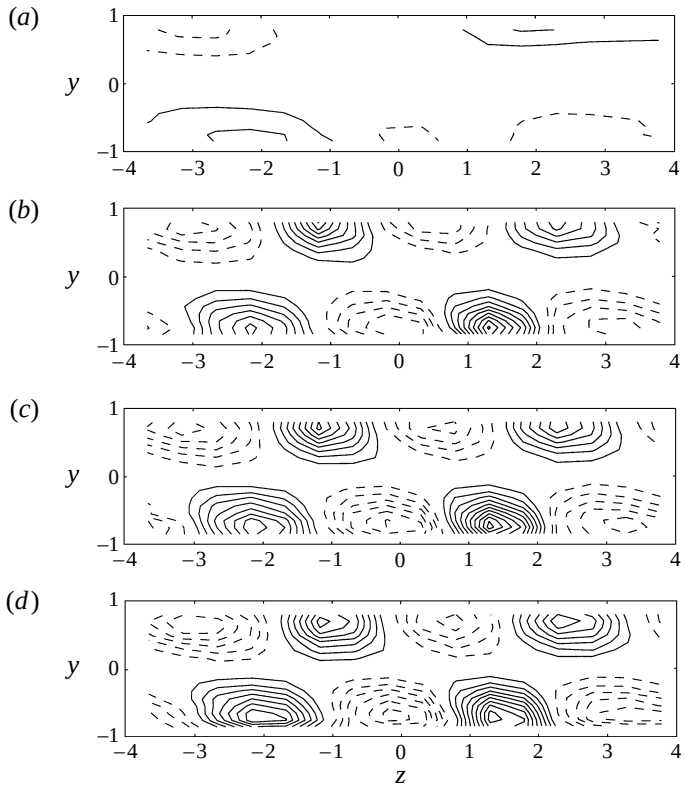

FIGURE 8. Contour plots of U_d in cross-stream planes for $Re = 2000$, $\omega = 0.33$ and $\phi = 45°$. (*a*) Measurements at $x = 15$; (*b*) $x = 40$; (*c*) $x = 50$; (*d*) $x = 65$. Contours : $\pm 1\,\%$, $\pm 2\,\%$... Negative contours are dashed.

Lundbladh (1994). However, all the features of oblique transition are still captured in the experiment, despite the difference compared to an ideal theoretical case. Some further discussion and comparison between experiments and simulations are presented in § 5.

4.2. *High-amplitude results*

With a low initial wave amplitude a large-amplitude stationary structure will develop but breakdown will not occur in the region of measurements. However, if the initial amplitude is increased the downstream development will change substantially. Figure 9 (*a–c*) shows the same plots as in figure 7 but for a high amplitude of the original waves. The maximum value (close to the ribbons) of $u_{r.m.s.,f_0}$ was 6.4 % and the data were measured at the same positions and with the same parameter settings as in figure 7.

Also here the initial development of the interaction gives rise to longitudinal streaks with about the same wavenumber as in the low amplitude case. The maximum amplitude of the streaks is now however, in the range of $\pm 20\,\%$. In the downstream part of the measurement region the streaks are less well defined. The time-dependent disturbance ($u_{r.m.s.}$) reach high amplitudes, of the order of 15 %, whereas disturbances around the fundamental frequency decay at the end of the measurement region suggesting a transfer of energy from the fundamental to other frequencies during the

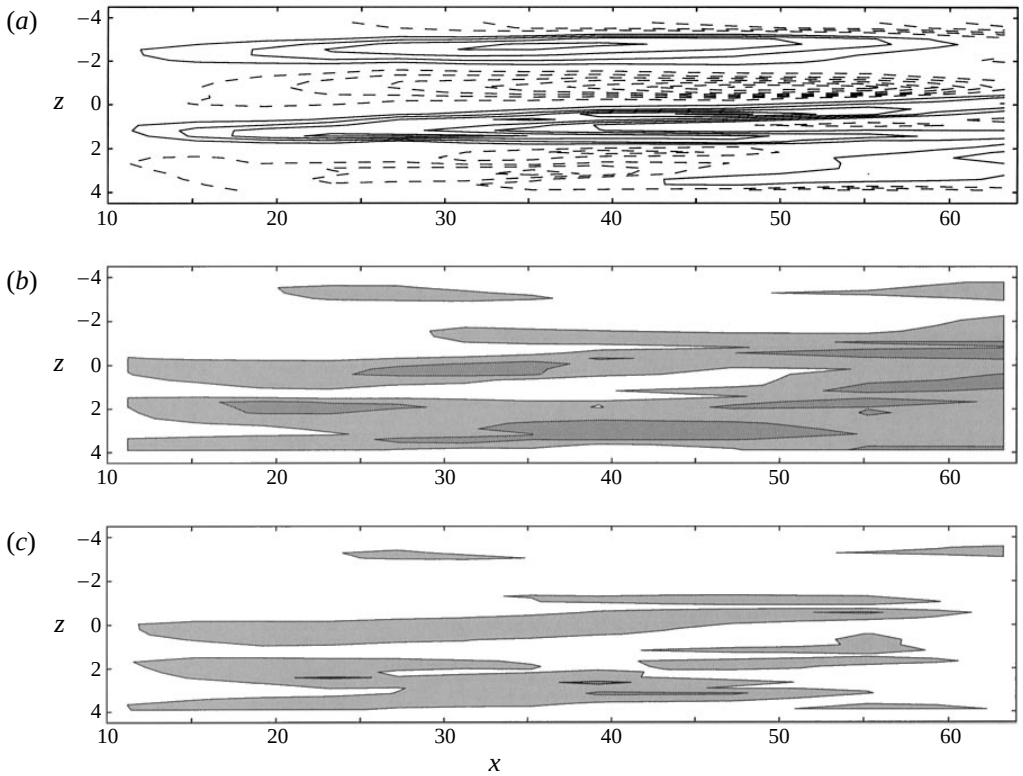

FIGURE 9. Contour plots in a streamwise–spanwise plane at $y = -0.75$, $Re = 2000$, $\omega = 0.33$ and $\phi = 45°$. (*a*) U_d, contours: $\pm 4\,\%$, $\pm 8\,\%$.; (*b*) $u_{r.m.s.}$, contours : $6\,\%$, $12\,\%$.; (*c*) $u_{r.m.s.f_0}$, contours: 6%, 12%... Negative contours are dashed.

transition stage. One explanation for the downstream observations may be that the streaks have started to oscillate in the spanwise direction.

As can be seen in figure 10 the structure of U_d in a cross-stream plane is similar to the one for the low-amplitude case but the amplitude is now larger. However, the main difference between a low and a high initial amplitude is seen in the downstream development of $u_{r.m.s.}$. Instead of decaying in the streamwise direction, as for a low amplitude, $u_{r.m.s.}$ grows and localized regions of high amplitude first appear close to the walls and then move towards the centreplane of the channel (see figure 11). These maxima appear mainly at positions between regions of positive and negative U_d but they are also observed inside regions with negative U_d (cf. figure 10). Initially the main contribution to $u_{r.m.s.}$ is from disturbances with the same frequency as the forcing signal to the ribbons, but further downstream the contribution from harmonics of the forcing signal is increasing. The positions of the maxima for the second harmonic are mainly concentrated in regions with negative U_d (not shown).

Figure 12 shows profiles of $\overline{U}$ and $u_{r.m.s.}$ measured at $z = 0.6$ (marked as dashed lines in figure 10). At this spanwise position $y < 0$ is a region with large spanwise gradients in U_d and $y > 0$ corresponds to a region of negative U_d. Initially the largest growth in $u_{r.m.s.}$ is seen to occur close to the lower wall and values near 15 % are reached at $x = 30$. Later the region of maximum amplitude is moving towards the

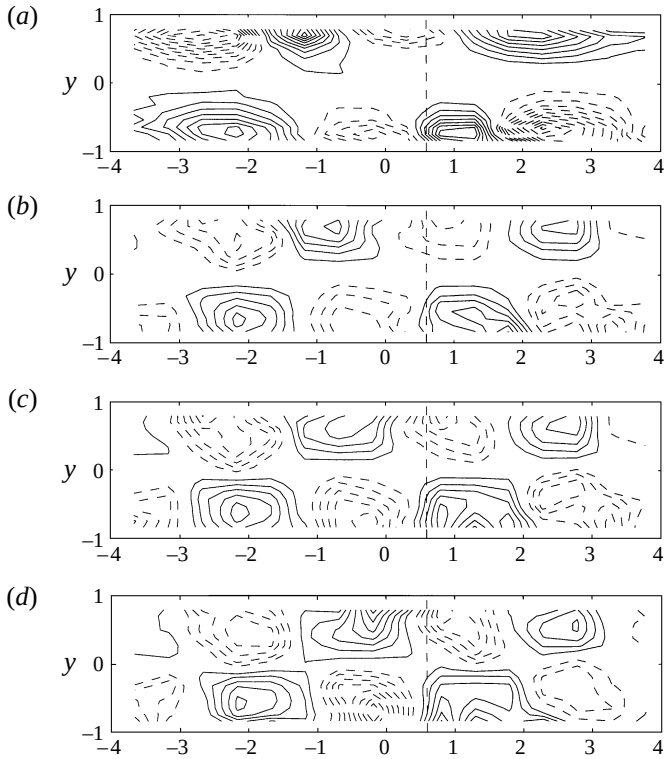

FIGURE 10. Contour plots of U_d in cross-stream planes for $Re = 2000$, $\omega = 0.33$ and $\phi = 45°$. (*a*) Measurements at $x = 15$; (*b*) $x = 40$; (*c*) $x = 50$; (*d*) $x = 65$. Vertical lines indicate spanwise position for y-profiles. (*a*) Contours are: $\pm 0.5\%$, $\pm 1\%$..; (*b–d*) contours are: $\pm 4\%$, $\pm 8\%$... Negative contours are dashed.

centre of the channel with increasing x and a strong growth is also seen for $y > 0$. At the last streamwise position the time-dependent disturbance ($u_{r.m.s.}$) is almost equally distributed through the central part of the channel which signifies the flow being close to transition.

To get more insight into the development of the disturbances it may be worthwhile to study the spectra in different regions of the flow. The sequence of spectra shown in figure 13 is taken with $\omega = 0.34$ at $y = -0.75$ and $z = 1.3$, which corresponds to a region of positive U_d. In this case the wave amplitude was about 5% and the wave angle was $\phi = 34°$, but the development was similar for $\phi = 45°$.

At the first streamwise position the amplitude of the fundamental and its first harmonics show clear peaks in the spectrum, but their amplitudes are relatively low compared to a spectrum obtained at a corresponding region with negative U_d (not shown). A pronounced growth of higher harmonics is observed to occur between $x = 50$ and $x = 58$, and at the last streamwise position the spectrum displays similar amplitudes for the fundamental frequency and its harmonics. One should be aware of the distinction between spectra obtained at different cross-stream regions. In a region with negative U_d a substantial filling of the spectrum is seen at $x = 65$, and also the peak amplitudes are larger than for the present region with positive U_d.

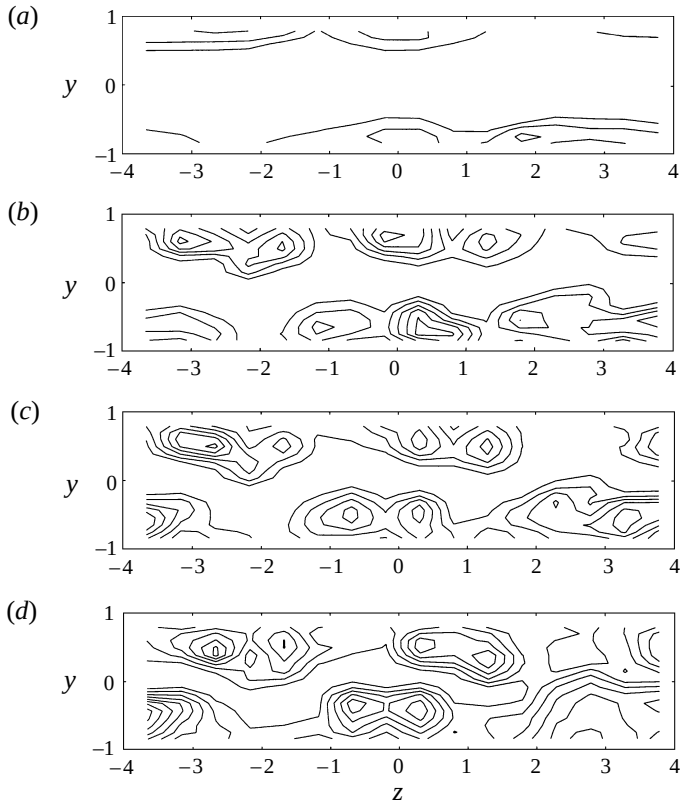

FIGURE 11. Contour plots of $u_{r.m.s.}$ in cross-stream planes for $Re = 2000$, $\omega = 0.33$ and $\phi = 45°$. (*a*) Measurements at $x = 15$; (*b*) $x = 40$; (*c*) $x = 50$; (*d*) $x = 65$. Contours are: 2.5%, 5%...

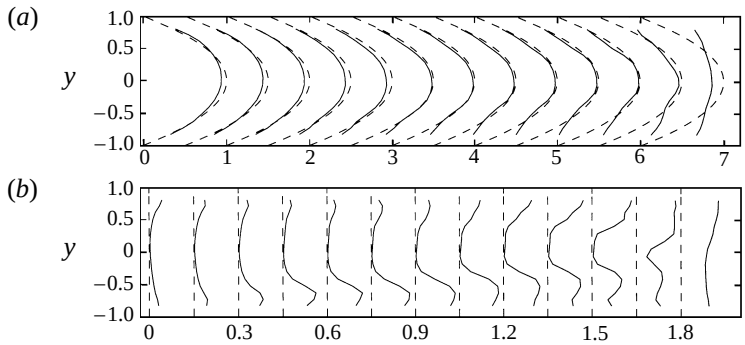

FIGURE 12. Measurements with $Re = 2000$, $\omega = 0.33$ and $\phi = 45°$ at $z = 0.6$ and $x = 10$, 14, 18, 22, 26, 30, 34, 38, 42, 46, 50, 58 and 66. (*a*) Wall-normal profiles of $\overline{U}$; (*b*) wall-normal profiles of $u_{r.m.s.}$. Dashed lines correspond to the parabolic profile and $u_{r.m.s.} = 0$, respectively.

4.3. *Amplitude evolution of Fourier modes*

In order to get further information about the oblique transition process it is useful to study how the disturbances evolve in the (ω, β)-plane. The present measurements were made at $y = 0.75$ by traversing the hot-wire probe in the spanwise direction over a total of 64 measurement positions with a spanwise separation between measurement

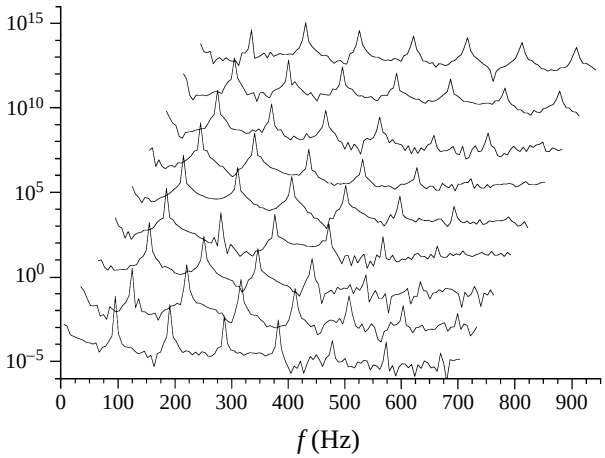

FIGURE 13. Amplitude spectra measured at $y = -0.75$, $z = 1.28$ and $x = 16$, 21, 26, 31, 36, 43, 50, 58 and 65 with $Re = 2000$, $\phi = 34^\circ$ and $\omega = 0.34$. Consecutive spectra are shifted 30 Hz and multiplied by 10^2.

points of $\Delta z = 0.2h$. The y-position was chosen to be close to the position of the maximum of $u_{r.m.s.,f_0}$. Fourier transforms of the time series (sampled with 2880 Hz) were made during the measurements and the Fourier components obtained by averaging 25 sets of phase-aligned data were stored on file. After completion of the measurements the energy in (ω, β)-modes was determined by performing a spanwise Fourier transform of the phase-aligned data. The energy is defined as the square of the absolute value of the normalized Fourier components, i.e. $E = |\hat{u}(\omega_m, \beta_n)|^2$.

Figure 14 (*a*) shows the result obtained with an amplitude of 1.6 % (corresponding to the low-amplitude results in § 4.1) for which breakdown did not occur. The notation used for the modes is $(\omega/\omega_0, \beta/\beta_0)$, where ω_0 and β_0 are the initial angular frequency and spanwise wavenumber, respectively. For comparison the decay rate for the $(1, 1)$-mode obtained from linear stability theory is also shown in the figure (dashed line).

From the figure it is seen that by the first streamwise measurement position the energy in the stationary mode denoted $(0, 2)$ is approximately the same as the energy in the forcing mode $(1, 1)$. Energy is transferred directly into the $(0, 2)$-mode through a nonlinear interaction between the initial $(1, \pm 1)$-modes. This mode then experiences a large transient growth and continues to grow for all positions but the growth rate decreases in the downstream direction. Also, the energy in the (1,3)-mode is seen to grow until $x \approx 28$ before it starts to decay. It can be observed that the decay of the $(1, 1)$-mode almost follows the damping obtained from a linear stability calculation for a single oblique wave. However, the decay is modified due to energy transfer between modes. When compared with figure 3 in Schmid, Lundbladh & Henningson (1994), here reproduced in figure 14 (*b*), the energy evolution obtained from the experiment is found to display a striking similarity with their spatial simulation. However, only a qualitative comparison can be expected, mainly because of different starting conditions, but also since the measurements are made at one wall-normal position and the simulation data stem from an integration through the whole channel. In both cases, after an initial stage of positive growth, all modes decay and transition does not occur.

If the amplitude of the forcing signal to the ribbons is increased the energy

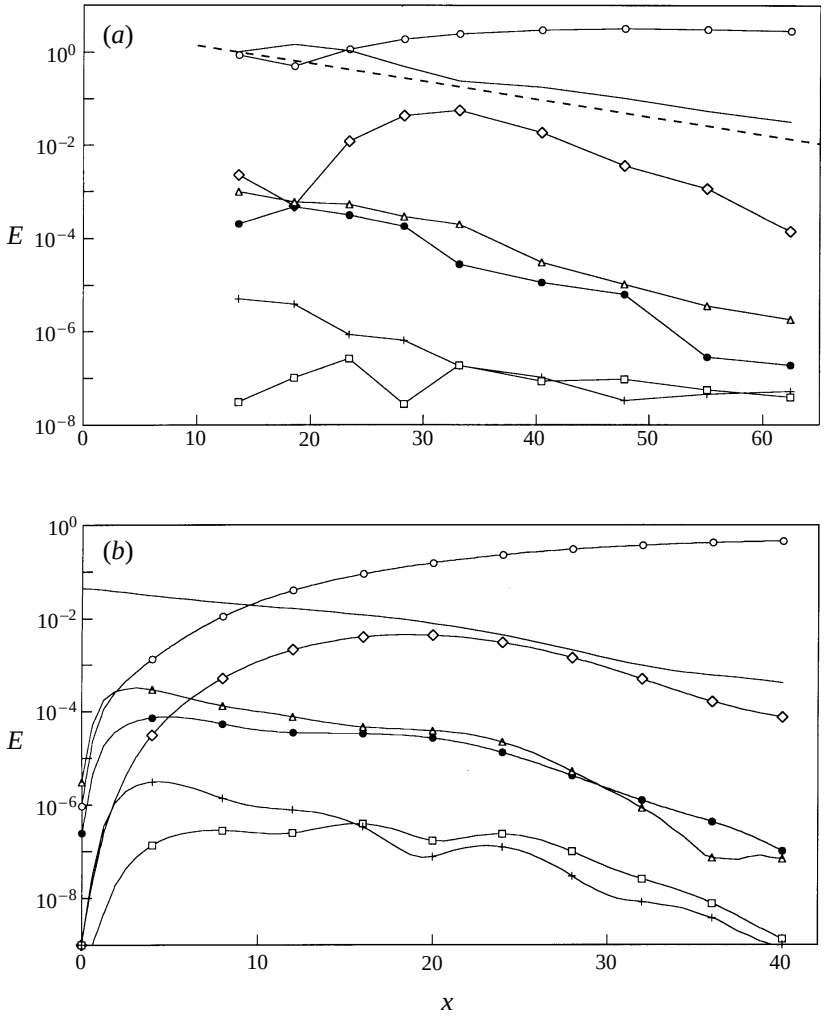

FIGURE 14. Energy in (ω, β)-modes at $Re = 2000$ and $\phi = 45°$ from (*a*) measurements for $\omega_0 = 0.33$ at $y = 0.75$ with a low initial amplitude and (*b*) spatial DNS by Schmid, *et al.* (1994). $(\omega/\omega_0, \beta/\beta_0) = :$ ——, (1,1); ○, (0,2); •, (2,2); △, (2,0); ◇, (1,3); □, (3,3); +, (3,1). The dashed line in (*a*) represent the decay rate obtained from a linear stability calculation for the (1,1)-mode. The data in (*a*) are normalized with the energy in the (1,1)-mode at the first measurement position.

evolution will change character and modes with frequencies that are harmonics of the forcing signal will start to grow. Figure 15 displays the energy evolution of (ω, β)-modes resulting from a high forcing amplitude (5%). As for the low-amplitude case the largest energy is found in the (0,2)-mode. The (1,1)-mode grows initially but then starts to decay at $x \approx 19$ and for this higher amplitude the energy in the (1,3)-mode almost reaches the same level as for (1,1). One can note that the large amplitude of the (1,3)-mode is clearly observed in physical space also, in the form of the double-peaks in $u_{r.m.s.}$ seen in figure 11. The main difference between the low and high amplitude cases is the strong growth of the higher harmonics in the high amplitude case, whereas for low amplitudes these harmonics always decayed.

Another way to illustrate the growth of the higher harmonics is to show the

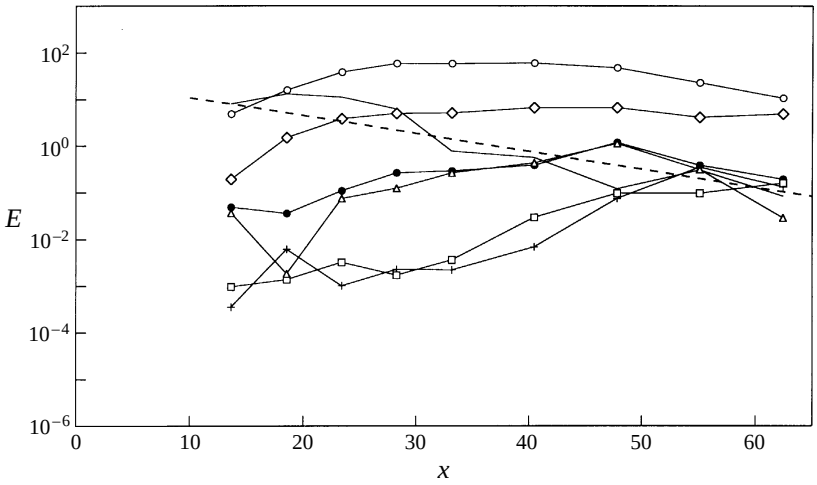

FIGURE 15. Energy in (ω, β)-modes from measurements with a high initial amplitude. Data are normalized with the energy in the (1,1)-mode at the first measurement position with a low initial amplitude (in figure 14*a*). Same notation as in figure 14.

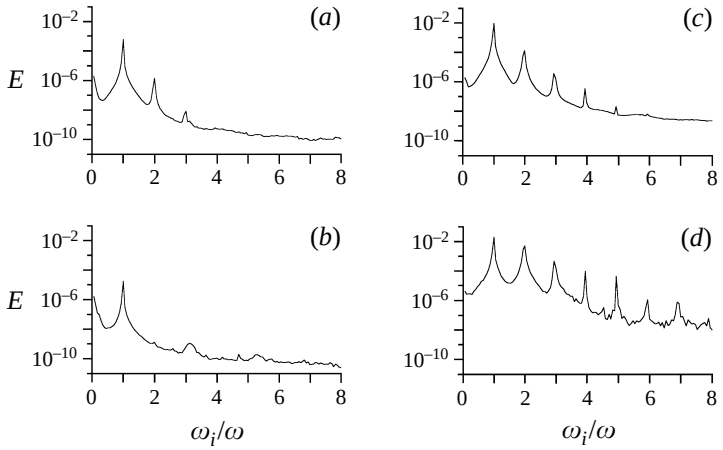

FIGURE 16. Energy density at $y = 0.75$ for $Re = 2000$, $\omega = 0.33$ and $\phi = 45°$: (*a*) low amplitude, $x = 12$; (*b*) low amplitude, $x = 60$; (*c*) high amplitude, $x = 12$; (*d*) high amplitude, $x = 60$.

spectra averaged over all spanwise wavenumbers. Figure 16 shows data from the same measurements as above at two streamwise positions, $x = 12$ and $x = 60$. The results were obtained by adding the Fourier components from all the spanwise wavenumbers for each frequency. Initially the spectra are similar both for the low- and high-amplitude cases with a dominant peak at the forcing frequency. For the higher amplitude a few more of the higher harmonics are observed but these are of very low-amplitude. At $x = 60$ the picture is however completely changed. For the low amplitude case only the forcing frequency is seen; however it has decayed slightly. For the high amplitude case on the other hand, both the fundamental and all harmonics have increased in amplitude: notable is that the second harmonic almost reaches the same amplitude as the fundamental. It can also be observed that the spectrum has

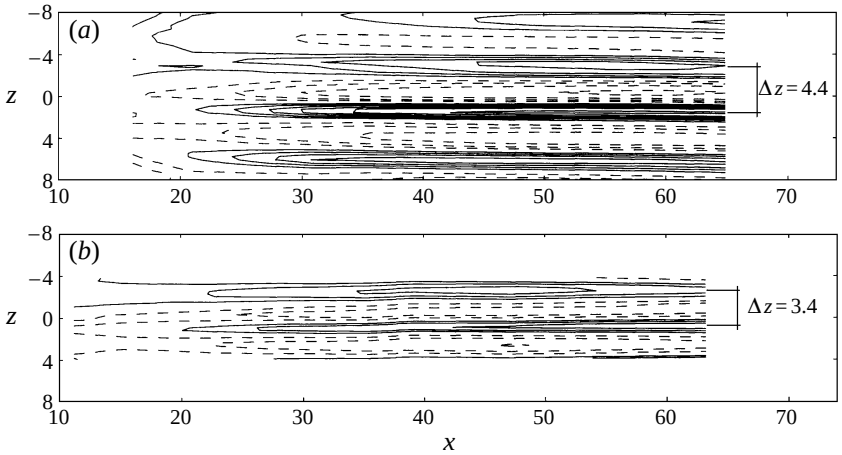

FIGURE 17. Contour plots of U_d in a streamwise–spanwise plane at $y = -0.75$ with $Re = 2000$ and $\omega = 0.33$. (*a*) $\phi = 34°$; (*b*) $\phi = 45°$. Contours: $\pm 1\,\%$, $\pm 2\%$. . . .

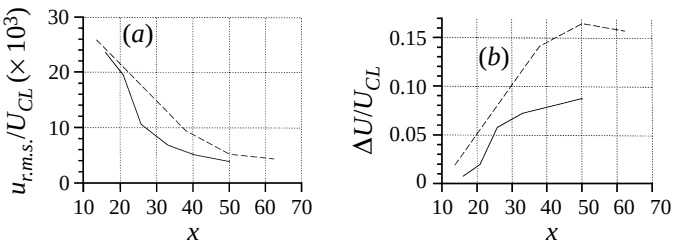

FIGURE 18. Evolution of: (*a*), $u_{r.m.s.}$; (*b*), ΔU for $Re = 2000$, and $\omega = 0.34$. ——, Wave angle is $\phi = 34°$; ——, wave angle is $\phi = 45°$.

started to become filled between the harmonics which is an indication that transition has started.

4.4. *Wave angle effect*

Theoretically it is clear that the non-linear interaction between a pair of oblique waves will result in the (0,2)-mode. This was confirmed in the experiment by using two different wave angles. Most of the measurements were made with an angle of 45° in order to be able to compare with numerical simulations. The other wave angle used was $\phi = 34°$ which should give a streak spacing that is 4/3 of the one obtained for $\phi = 45°$. The difference in streak spacing can be observed in figure 17, which shows contour plots of U_d in streamwise–spanwise planes obtained at two different wave angles.

Figure 18 displays the evolution of $u_{r.m.s.}$ and ΔU for data obtained from measurements at the two wave angles with an initial amplitude in the low-amplitude regime. The data were obtained by extracting the maximum $u_{r.m.s.}$ value from a spanwise position near $z = 0$ and the streak amplitude (ΔU) was defined to be the difference between the maximum and minimum mean velocity near $z = 0$ for a y-position where the maximum $u_{r.m.s.}$ value was found. It is seen that a wave angle of $\phi = 45°$ results in a larger streak amplitude than what is found for $\phi = 34°$, but no large differences are seen in the $u_{r.m.s.}$ values (they decay from the same level with the same rate). The results indicate that the smaller spanwise wavelength is less stable; however,

small differences in the initial amplitudes of the waves may also play a role. In order to investigate the influence of β on the stability of the streaks another method to produce streaks should probably be used (such as suction through small holes at the wall with different spacing).

A similar result was obtained in the temporal numerical simulations by Schmid & Henningson (1992) who found that an increasing wave angle resulted in a decrease in the time taken to reach the energy peak. Since the energy amplification factor remained constant this resulted in an increasing growth rate.

5. Summary and discussion

The interaction of two oblique waves gives rise to the formation of streamwise-oriented vortices, which generate stationary streamwise streaks of high and low velocity. These streaks may grow, even if the flow is subcritical to modal disturbances. If the streak amplitude becomes high enough secondary instabilities may come into play whereupon breakdown and finally transition to turbulence occurs.

In an experiment streaky structures may be obtained for many different types of forcing, for instance localized suction or injection through the wall (continuously or pulse-wise), localized roughness elements or from free-stream turbulence. If one is attempting to study the transition process where streaky structures are involved the use of oblique waves to generate the streaky structures has an advantage since the initial conditions can be more accurately described than for instance those occurring at a roughness element. The interaction of oblique waves may also occur naturally, e.g. between two wave packets or between oblique waves in supersonic boundary layers (in the supersonic case oblique waves may be the most amplified).

From the measurements of the flow field resulting from the interaction between a pair of oblique waves we were able to distinguish two regimes which are strongly related to the amplitude of the initial waves. The first regime is obtained at low amplitudes and gives streaks which reach a maximum after which they decay. In this regime higher modes decay and far downstream only the streaks remain. In this paper we describe experiments at $Re = 2000$ where the streaks reach an amplitude of $\pm 4 - 5\%$ around $x = 45$ before they slowly decay downstream; however they can still be observed at $x \approx 125$. Despite the finite amplitude of the streaks, modes with non-zero frequency decay (except for a short initial growth of the (1,3)-mode). Other experiments at the same Reynolds number show that we observe a similar behaviour for streak amplitudes up to 2 to 3 times higher.

For the second, high-amplitude, regime on the other hand, the non-zero frequency modes are amplified when the streak amplitude reaches a threshold of about $\pm 12 - 15\%$. The $(0, 2)$-mode is still dominating and for the present experiment the maximum streak amplitude is now around $\pm 20\%$. As the higher modes grow downstream the streaks become less regular.

When comparing the present experiment with the scenario proposed by Berlin *et al.* (1994) it is clear that they have many features in common. The streaks are generated both for low and high initial amplitudes, and if the streak amplitude becomes large higher frequency–wavenumber components grow rapidly and the flow goes towards breakdown.

The first stage in the proposed oblique transition scenario is the formation of streamwise vortices. An analysis is presented in the Appendix which shows that the interaction of two oblique waves forces streamwise vorticity with half the spanwise

wavelength of the original waves. In order to experimentally verify the formation of the vortices it is not sufficient to study the streamwise velocity component, but one would need to have information about the other velocity components as well. An attempt was made to measure the spanwise velocity component in a region close to the intersection of the ribbons ($x < 20$). The spanwise velocity component (W) was obtained from measurements utilizing one slanted hot-wire probe (45°) and one straight probe. The W-component was then determined by subtracting the velocity given by the straight probe from the one obtained by the slanted wire probe from measurements at the same position. However, no conclusive data could be obtained except that the spanwise velocity was less than 1% of U_{CL}, which shows that the strength of the vortices is small.

One can both from the results shown in the Appendix and from symmetry reasoning argue that streaks of high velocity should occur at the same z-position on both sides of the channel and vice versa for low-velocity streaks. In the experiments this is not the case: for the low-amplitude case the symmetry properties are a mixture; for the high-amplitude case there is almost complete anti-symmetry with respect to the centreplane ($y = 0$) for large x. One may hypothesize that the symmetric arrangement of high and low-velocity regions is inherently unstable and that an initial asymmetry will become more pronounced the higher the amplitude of the streaks.

The generation of TS-waves in an experiment will always give rise to a wave which is an approximation of an ideal TS-wave. For instance, initially it will typically contain higher modes, and it will also take some downstream distance before it has been established throughout the boundary layer or channel. The present experiments seem to indicate that there is a slight difference in amplitude between the channel halves even for large downstream distances; however the wave characteristics are still close to the theoretical ones. In order to investigate some of the details of ribbon-induced TS-waves, Elofsson & Lundbladh (1994) made numerical simulations with a spatial version of the code by Lundbladh, Henningson & Johansson (1992). The action of the vibrating ribbons was modelled by adding time-periodic volume forces to the Navier–Stokes equations in the regions occupied by the ribbons. The amplitude of the volume forces was adjusted to get the same level of $u_{r.m.s.}$ at $(x, y, z) = (15, -0.75, 0)$ as was observed in a reference experiment. Several grids were tested with up to $256 \times 49 \times 320$ spectral modes in the streamwise, wall-normal and spanwise directions, respectively. Figure 19 is reproduced from Elofsson & Lundbladh and shows a comparison between measurements (a) and simulations (b). In the figure U_d is plotted on an (x, z)-plane at $y = -0.75$ and the agreement between experiments and simulations is seen to be close. From the simulations it was shown that with the arrangement of the present experiment a non-symmetry with respect to the centreplane would occur, which was also observed in the experiment (see § 4.1).

5.1. *Relation to bypass transition*

In many situations the transitional Reynolds number is lower than the critical Reynolds number for which linear wave disturbances grow exponentially. In these cases one generally denotes the transition as 'bypass transition'. Originally Morkovin (1969) stated that "Apparently, . . . , we can bypass the TS mechanism altogether if we can replace it with another strongly amplifying mechanism–". In his case he referred to inflectional instability, but bypass usually refers to all transition scenarios which do not start with amplified TS-waves. One example is transition which initially depends on algebraically growing disturbances.

In Klingmann's (1992) experiment the appearance of large-amplitude streaks was

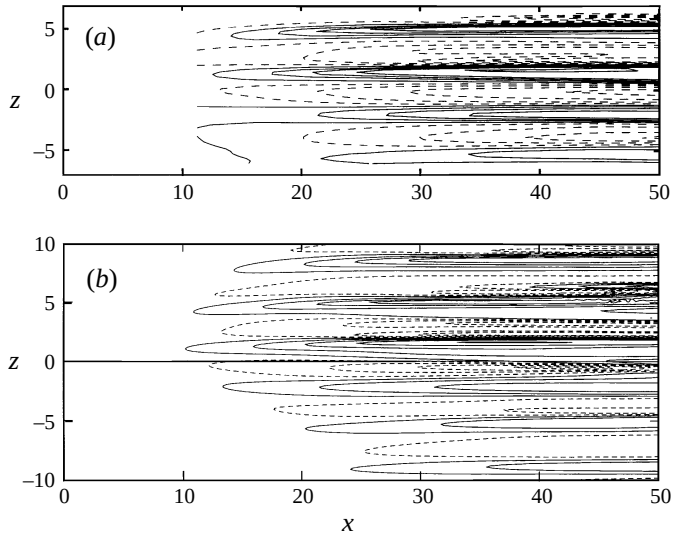

FIGURE 19. From Elofsson & Lundbladh (1994). U_d in an (x, z)-plane at $y = -0.75$ for $Re = 2000$, $\omega = 0.34$ and $\phi = 45°$. (*a*) Experimental results and (*b*) simulation results. Contour spacing is 0.05.

observed when introducing a localized (in time as well as space) disturbance from a small hole in one wall. At low amplitudes they decayed after an initial growth whereas large-amplitude disturbances gave rise to turbulent spots. There are many similarities between the current experiments and Klingmann's investigation. However, the use of a pair of vibrating ribbons provides a controlled way to generate the initial streaky disturbance as well as subsequent higher modes. In our case the oblique waves are exponentially decaying and the growth is first seen as a growth of the streaks (i.e. transient growth). Hence, the oblique transition scenario may be classified as one form of bypass transition. In fact, as discussed above, there are a number of disturbances that will create streaks, and it seems plausible that when such streaks have formed, algebraic growth will be responsible for their amplification and that the breakdown is not too sensitive to the actual origin of the streaks.

An interesting aspect of three-dimensional disturbance growth in the case of a laminar boundary layer on a flat plate is transition under the influence of free-stream turbulence. Also in this case the initial development gives streaky structures (see e.g. Westin *et al.* 1994 and Luchini 1996). Flow visualization has indicated that a wavy type of secondary instability on the streaks is the first step in the breakdown process to fully turbulent flow (Matsubara & Alfredsson 1995).

5.2. *Summary of major results*

The initial part of the current investigation concerned experimental verification of the linear stability of two-dimensional and three-dimensional TS-waves in plane Poiseuille flow. The experiments extend the results of Nishioka *et al.* (1975) and are in excellent correspondence with linear theory regarding phase speed, growth rate (or rather decay) and amplitude and phase distributions.

The interaction of two oblique waves was found to give rise to stationary streamwise-oriented streaks of high and low velocity, which initially grow in amplitude. The spanwise wavenumber is twice the wavenumber of the oblique waves.

For low initial amplitudes the streaks reach a maximum whereupon they decay.

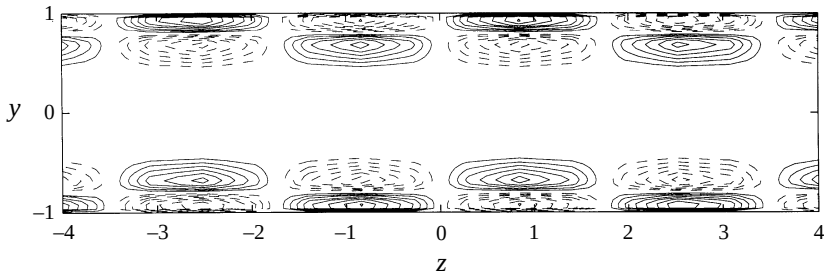

FIGURE 20. Net contribution from nonlinear forcing terms (averaged over one streamwise wavelength). $Re = 2000$, $\phi = 45°$ and $\omega = 0.33$. Amplitude is arbitrary.

From the experimental data it was possible to obtain the development of various (ω,β)-modes and in this case all modes were found to decay.

For a high initial amplitude of the oblique waves the streaks grow to high amplitude but in this case other modes also grow strongly. It is clearly seen that high-frequency modes are mainly amplified in regions of large spanwise shear, indicating that the spanwise inflectional profiles are important for this growth. For large x the dominating mode is $(1, 3)$ which in physical space is seen as double-peaks in $u_{r.m.s.}$, centred around regions with negative U_d.

From the three last points listed above one can conclude that the present study has, for the first time, verified the oblique transition scenario in a physical experiment.

Fruitful discussions with Dan Henningson and co-workers are gratefully acknowledged. This work was supported by the Swedish Research Council for Engineering Sciences (TFR).

Appendix

The interaction of two oblique waves gives rise to streamwise vortices. This may not be obvious but can be seen from the vorticity equation. The vorticity equation may be written

$$\frac{\mathrm{D}\overline{\boldsymbol{\omega}}}{\mathrm{D}t} = (\overline{\boldsymbol{\omega}} \cdot \nabla)\overline{\boldsymbol{u}} + \nu\nabla^2\overline{\boldsymbol{\omega}}.$$

Now consider a parallel shear flow where the basic flow is given by $(U(y), 0, 0)$ and the fluctuating velocity components are (u, v, w). By taking the x-component of the vorticity equation we get

$$\left(\frac{\partial}{\partial t} + U\frac{\partial}{\partial x}\right)\omega_x = -U'\frac{\partial w}{\partial x} + \nu\nabla^2\omega_x - (\overline{\boldsymbol{u}} \cdot \nabla)\boldsymbol{\omega}_x + (\overline{\boldsymbol{\omega}} \cdot \nabla)u.$$

The two first terms on the right-hand side are linear in the disturbance quantities and give changes in ω_x due to vortex stretching and viscous diffusion respectively. The two last terms are nonlinear in the disturbance quantities and are the source for the nonlinear interaction, i.e. they are forcing terms for the higher modes of ω_x. By using the velocity distribution for two oblique waves (obtained from (2.5), (2.6) and continuity) it is possible to explicitly calculate the forcing terms. By averaging the contributions from the different terms over one period in time one obtains the forcing shown in figure 20. It is clear that the forcing has a pattern of regions of

alternating sign, which would tend to give rise to streamwise counter-rotating vortices. By studying the individual terms it is found that $\omega_y \partial u/\partial y$ and $\omega_z \partial u/\partial z$ give the largest contributions.

REFERENCES

Berlin, S., Lundbladh, A. & Henningson, D. S. 1994 Spatial simulations of oblique transition in a boundary layer. *Phys. Fluids* **6**, 1949–1951.

Boiko, A. V., Westin, K. J. A., Klingmann, B. G. B., Kozlov, V. V. & Alfredsson, P. H. 1994 Experiments in a boundary layer subjected to free stream turbulence. Part 2. The role of TS-waves in the transition process. *J. Fluid Mech.* **281**, 219–245.

Butler, K. M. & Farrell, B. F. 1992 Three-dimensional optimal perturbations in viscous shear flow. *Phys. Fluids* A **4**, 1637–1650.

Corke, T. C. & Mangano, R. A. 1989 Resonant growth of three-dimensional modes in transitional Blasius boundary layers. *J. Fluid Mech.* **209**, 93–150.

Ellingsen, T. & Palm, E. 1975 Stability of linear flow. *Phys. Fluids* **18**, 487–488.

Elofsson, P. A. & Alfredsson, P. H. 1995 Experiments on nonlinear interaction between oblique Tollmien-Schlichting waves. In *Laminar-Turbulent Transition* (ed. R. Kobayashi), pp. 465–472. Springer.

Elofsson, P. A. & Lundbladh, A. 1994 Ribbon induced oblique transition in plane Poiseuille flow. In *Bypass Transition - Proceedings from a Mini - Workshop, Stockholm* (ed. D. S. Henningson), pp. 29–41. *TRITA-MEK, Tech. Rep.* 1994:14.

Gaster, M. 1975 A theoretical model for the development of a wave packet in a laminar boundary layer. *Proc. R. Soc. Lond.* A **347**, 271–289.

Gustavsson, L. H. 1991 Energy growth of three-dimensional disturbances in plane Poiseuille flow. *J. Fluid Mech.* **224**, 241–260.

Henningson, D. S. 1995 Bypass transition and linear growth mechanisms. In *Advances in Turbulence V* (ed. R. Benzi), pp. 190–204. Kluwer.

Henningson, D. S., Lundbladh, A. & Johansson, A. V. 1993 A mechanism for bypass transition from localized disturbances in wall bounded shear flows. *J. Fluid Mech.* **250**, 169–207.

Herbert, T. 1983 Secondary instability of plane channel flow to subharmonic three-dimensional disturbances. *Phys. Fluids* **26**, 871–874.

Kachanov, Y. S. & Levchenko, V. Y. 1984 The resonant interaction of disturbances at laminar turbulent transition in a boundary layer. *J. Fluid Mech.* **138**, 209–247.

Kachanov, Y. S. & Michalke, A. 1994 Three-dimensional instability of flat-plate boundary-layers: Theory and experiment. *Eur. J. Mech.* B/*Fluids* **13**, 401–422.

Klebanoff, P. S., Tidstrom, K. D. & Sargent, L. M. 1962 The three-dimensional nature of boundary layer instability. *J. Fluid Mech.* **12**, 1–34.

Klingmann, B. G. B. 1992 On transition due to three-dimensional disturbances in plane Poiseuille flow. *J. Fluid Mech.* **240**, 167–195.

Klingmann, B. G. B., Boiko, A. V., Westin, K. J. A., Kozlov, V. V. & Alfredsson, P. H. 1993 Experiments on the stability of Tollmien-Schlichting waves. *Eur. J. Mech.* B/*Fluids* **12**, 493–514.

Landahl, M. T. 1980 A note on an algebraic instability of inviscid parallel shear flows. *J. Fluid Mech.* **98**, 243–251.

Luchini, P. 1996 Reynolds-number-independent instability of the boundary layer over a flat surface. *J. Fluid Mech.* **327**, 101–115.

Lundbladh, A., Henningson, D. S. & Johansson, A. V., 1992 An efficient spectral integration method for the solution of the Navier-Stokes equations. *FFA-TN* 1992-28. Aeronautical Research Institute of Sweden, Bromma.

Lundbladh, A., Schmid, P. J., Berlin, S. & Henningson, D. S., 1994 Simulations of bypass transition for spatially evolving disturbances. *AGARD-CP*-551.

Matsubara, M. & Alfredsson, P. H. 1995 Free stream turbulence induced boundary layer transition. *Bull. Am. Phys. Soc.* **40** (12), 1956.

Mayer, E. W. & Reshotko, E. 1997 Evidence for transient disturbance growth in a 1961 pipe-flow experiment. *Phys. Fluids* **9**, 242–244.

Morkovin, M. V. 1969 The many faces of transition. In *Viscous Drag Reduction* (ed. C. S. Wells). Plenum.

Nishioka, M., Iida, S. & Ichikawa, Y. 1975 An experimental investigation of the stability of plane Poiseuille flow. *J. Fluid Mech.* **72**, 731–751.

Reddy, S. C., Schmid, P. J., Baggett, J. S. & Henningson, D. S. 1998 On stability of streamwise streaks and transition tresholds in plane channel flows. *J. Fluid Mech.* (accepted).

Saiki, E. M., Biringen, S., Danabasoglu, G. & Streett, C. L. 1993 Spatial simulation of secondary instability in plane channel flow: comparison of K- and H-type disturbances. *J. Fluid Mech.* **253**, 485–507.

Schlichting, H. 1979 *Boundary Layer Theory*. McGraw-Hill.

Schmid, P. J. & Henningson, D. S. 1992 A new mechanism for rapid transition involving a pair of oblique waves. *Phys. Fluids* A **4**, 1986–1989.

Schmid, P. J., Lundbladh, A. & Henningson, D. S. 1994 Spatial evolution of disturbances in plane Poiseuille flow. In *Transition, Turbulence and Combustion, Volume I* (ed. M. Y. Hussaini, T. B. Gatski & T. L. Jackson), pp. 287–297. Kluwer.

Schubauer, G. B. & Skramstad, H. K. 1947 Laminar boundary layer oscillations and the stability of laminar flow. *J. Aero. Sci.* **14**, 69–78.

Singer, B. A., Reed, H. L. & Ferziger, J. H. 1989 The effects of streamwise vortices on transition in the plane channel. *Phys. Fluids* A **1**, 1960–1971.

Trefethen, L. N., Trefethen, A. E., Reddy, S. C. & Driscoll, T. A. 1993 Hydrodynamic stability without eigenvalues. *Science* **261**, 578–584.

Waleffe, F. 1997 On a self-sustaining process in shear flows. *Phys. Fluids* **9**, 883–900.

Westin, K. J. A., Boiko, A. V., Klingmann, B. G. B., Kozlov, V. V. & Alfredsson, P. H. 1994 Experiments in a boundary layer subjected to free-stream turbulence. Part 1. Boundary layer structure and receptivity. *J. Fluid Mech.* **281**, 193–218.

Wiegel, M. 1996 Experimentelle Untersuchung von kontrolliert angeregten dreidimensionalen Wellen in einer Blasius-Grenzschicht. PhD thesis, TH Hannover.

Zang, T. A. & Krist, S. E. 1989 Numerical experiments on stability and transition in plane channel flow. *Theoret. Comput. Fluid Dyn.* **1**, 41–64.